Steel and Composite Structures, *Vol. 20, No. 4 (2016) 749-776*
DOI: http://dx.doi.org/10.12989/scs.2016.20.4.749

Performance based design approach for multi-storey concentrically braced steel frames

Suhaib Salawdeh [1,2a] and Jamie Goggins [*1,2,3]

[1] *Civil Engineering*, *College of Engineering & Informatics*, *National University of Ireland*, *Galway*, *Ireland*
[2] *Centre for Marine and Renewable Energy Ireland* (*MaREI*), *Galway*, *Ireland*
[3] *Ryan Institute*, *Galway*, *Ireland*

(*Received September 16, 2015, Revised November 27, 2015, Accepted February 24, 2016*)

Abstract. In this paper, a Performance Based Design (PBD) approach is validated for multi-storey concentrically braced frame (CBF) systems. Direct Displacement Based Design (DDBD) procedure is used and validated by designing 4- and 12-storey CBF buildings. Nonlinear time history analysis (NLTHA) is used to check the performance of the design methodology by employing different accelerograms having displacement spectra matching the design displacement spectrum. Displacements and drifts obtained from NLTHA are found to fall within the design displacement limits used in the DDBD procedure. In NLTHA, both tension and compression members are found to be resisting the base shear, F_b, not only the tension members as assumed in the design methodology and suggested by Eurocode 8. This is the reason that the total F_b in NLTHA is found to be greater than the design shear forces. Furthermore, it is found that the average of the maximum ductility values recorded from the time history analyses for the 4-and 12-storey buildings are close to the design ductility obtained from the DDBD methodology and ductility expressions established by several researchers. Moreover, the DDBD is compared to the Forced Based Design (FBD) methodology for CBFs. The comparison is carried out by designing 4 and 12-storey CBF buildings using both DDBD and FBD methodologies. The performance for both methodologies is verified using NLTHA. It is found that the F_b from FBD is larger than F_b obtained from DDBD. This leads to the use of larger sections for the structure designed by FBD to resist the lateral forces.

Keywords: codified approach; concentrically braced frames; design methodology; direct displacement based design; steel

1. Introduction

Eurocode 8 (CEN 2004b) prescribes the force based design (FBD) methodology for the seismic design of structures. In FBD, lateral displacements are checked at the end of the design. If the lateral displacements were more than the design code limits, redesign should be carried out, which consumes time and causes unimportant redundancies for designers. On the other hand, the direct displacement based design (DDBD) procedure starts by considering a design displacement depending upon the drift limit. After that, the DDBD calculate the strength required to maintain this displacement avoiding the repetitions needed in FBD (Calvi and Sullivan 2009, Priestley *et al*.

*Corresponding author, Ph.D., E-mail: Jamie.goggins@nuigalway.ie
[a] Ph.D., E-mail: Suhaib.salawdeh@nuigalway.ie

http://www.techno-press.org/?journal=scs&subpage=6 ISSN: 1229-9367 (Print), 1598-6233 (Online)

2007).

Salawdeh (2012) validated a DDBD methodology for single storey concentrically braced frame (CBF) structures. To do so, he used physical shake table tests (Elghazouli *et al*. 2005) and numerical models. The NLTHA was validated in two stages. Firstly, a robust numerical model for a brace element, which is the main element to dissipate energy during seismic actions, is developed using pseudo dynamic cyclic tests (Salawdeh and Goggins 2013). This numerical model took into account fatigue that affects the brace elements and was advanced to represent a single-storey CBF structures by validating it to several shake table tests (Goggins and Salawdeh 2012). In this paper, the validity of a direct displacement based design (DDBD) procedure for multi-storey structures is checked by comparing its performance to NLTHA extended from the numerical model developed by Goggins and Salawdeh (2012). In this procedure, the inelastic behaviour is permitted for brace elements in order to dissipate energy induced from seismic actions through yielding in tension and buckling in compression. Beams and columns are designed to behave elastically. Fundamentals of the DDBD procedure for frames are taken from Priestley *et al*. (2007) and an equivalent viscous damping (EVD) model developed specifically for CBF by Wijesundara *et al*. (2011) is used. In the following section, a brief explanation of the DDBD procedure for CBF will be presented. Then, two case study building structures with four and eight stories will be designed using the DDBD procedure. These buildings will be validated using NLTHA by employing eight different accelerograms with displacement spectra matching the design displacement spectrum.

Current design procedures such as EC8 (CEN 2004b) use forced based design (FBD). Thus, two CBF buildings are designed using the FBD approach outlined in EC8 8 (CEN 2004b) and then the performance is gauged with NLTH analyses and compared with the DDBD solution.

2. DDBD procedure for CBFs

The design process starts by representing the multi degree of freedom (MDOF) system in the form of an equivalent single degree of freedom (SDOF) system with an effective mass at an effective height. Furthermore, DDBD characterizes the structure by the secant stiffness at the maximum displacement with a level of equivalent viscous damping, and then the base shear can be found and distributed to the floors, as will be explained in the next sub-sections.

2.1 Design storey displacements

The main concept of the DDBD procedure is to design the structure for a specified target displacement. Della Corte and Mazzolani (2008) proposed a drift shape for MDOF chevron CBFs taking into account axial deformations of columns and braces, as well as beam flexural deformations due to the unbalanced vertical force transmitted by the tension and compression braces, as the following

$$\theta_{i,d} = \frac{v^r_{i,d} - v^l_{i,d}}{L} + \frac{2\varepsilon^{tension}_{i,d}}{\sin 2\alpha} + \frac{v_{b,i,d}}{h_i}\tan\alpha + \frac{\varepsilon^r_{c,i,d} - \varepsilon^l_{c,i,d}}{2}\tan\alpha \quad (1)$$

where $\theta_{i,d}$ is the design drift, $v^r_{i,d}$ and $v^l_{i,d}$ are vertical displacements at the base of the *i*-th storey right and left column, respectively, which are due to elongation or shortening of columns from the first to the $(i–1)^{th}$ storey, L is the braced bay length, α is the angle of the brace on the horizontal

axis, $\varepsilon_{i,d}^{tension}$ is the tension brace axial strain at the i^{th} storey, $v_{b,i,d}$ is the beam mid-span vertical deflection at the i^{th} storey, h_i is the i-th storey height, $\varepsilon_{c,i,d}^{r}$ and $\varepsilon_{c,i,d}^{l}$ are the right and left column axial strains, respectively, at the i^{th} storey. As shown in Eq. (1), which represents chevron CBFs drifts, it is complicated and having many different variables. A simpler equation, suggested by Priestley *et al*. (2007), that can represent the displacement shape of CBFs is used. These expressions, given in Eqs. (2) and (3), were found to be reliable by several researchers (Medhekar and Kennedy 2000a, b, Moghaddam and Hajirasouliha 2006, Wijesundara 2009, Wijesundara *et al*. 2009) who conducted dynamic analysis of CBFs. The design storey displacements of the CBF, Δ_{Di}, can be obtained from a linear displacement pattern which depends upon the normalised inelastic mode shape, δ_i, and the displacement of the critical storey, Δ_C.

The inelastic mode shape can be found by the following equations

$$\text{For} \quad n \leq 4: \qquad \delta_i = \frac{H_i}{H_n} \tag{2}$$

$$\text{For} \quad n > 4: \qquad \delta_i = \frac{4}{3}\left(\frac{H_i}{H_n}\right)\left(1 - \frac{H_i}{4H_n}\right) \tag{3}$$

where n is the total number of storeys, i is the storey number, H_i is the height of the i^{th} level above foundation level and H_n is the height of the roof above foundation level. Priestley *et al*. (2007) suggested to use Eq. (2) for CBFs regardless of the number of storeys in the frame. However, using Eq. (2) for structures with up to 4 storeys and Eq. (3) for structures with more than 4 storeys gave satisfactory results, as will be discussed in the validation part of this paper.

The design storey displacements, Δ_{Di}, can be obtained from the following equation

$$\Delta_{Di} = \delta_i \left(\frac{\Delta_C}{\delta_C}\right) \tag{4}$$

where Δ_C is the displacement of the critical storey and δ_C is the normalised inelastic mode shape of the critical storey. The critical storey is normally the first storey level.

Calvi and Sullivan (2009) proposed an approach to include an allowance for higher mode amplification of drift, reducing the design floor displacements in Eqs. (2) and (3) by a drift reduction factor, ω_θ, as the following

$$\omega_\theta = 1.15 - 0.0034H_n \leq 1 \tag{5}$$

However, this approach is not used for this study. In order to account for the higher mode effects, 10% of the base shear force is allocated to the roof level and the remaining 90% of the base shear force is distributed to all floor levels, including the roof, in proportion to the product of mass and displacement, which will be explained on Section 2.7.

2.2 Equivalent SDOF system characteristics

With the knowledge of the displacement profile, it is possible to obtain various equivalent SDOF properties of the structure (Priestley *et al*. 2007). The equivalent SDOF design displacement, Δ_D, which is related to the storey displacements is given by

$$\Delta_D = \frac{\sum m_i \Delta_{Di}^2}{\sum m_i \Delta_{Di}} \tag{6}$$

where m_i is the mass at the height, H_i, associated with displacement, Δ_i. The effective mass, m_e, can be found by

$$m_e = \frac{\sum m_i \Delta_{Di}}{\Delta_D} \tag{7}$$

and the effective height, H_e, of the SDOF structure is given by

$$H_e = \frac{\sum m_i \Delta_{Di} H_i}{\sum m_i \Delta_{Di}} \tag{8}$$

2.3 Design displacement ductility

The design displacement ductility, μ, is found by dividing the design displacement, Δ_D, by the yield displacement, Δ_y, as the following

$$\mu = \frac{\Delta_D}{\Delta_y} \tag{9}$$

where the equivalent SDOF yield displacement, Δ_y, related to the storey yield displacements can be found by

$$\Delta_y = \frac{\sum m_i \Delta_{yi}^2}{\sum m_i \Delta_{yi}} \tag{10}$$

where Δ_{yi} is the yield displacement at the i^{th} floor. This displacement is the lateral drift required to yield the brace and the elastic column deformation at the moment the brace yields, which can be obtained from

$$\Delta_{yi} = \sum_{j=1}^{i} \left(\frac{\varepsilon_{br,y}}{\sin\alpha \cos\alpha} h_j + \varepsilon_{col,y} h_j \tan\alpha \right) \tag{11}$$

where $\varepsilon_{br,y}$ is the brace axial strain, α is angle of the brace with the horizontal axis, h_j is the storey height and $\varepsilon_{col,y}$ is the column axial strain. The derivation of Eq. (11) can be found in Della Corte and Mazzolani (Della Corte *et al*. 2010) and Wijesundara (Wijesundara *et al*. 2011).

2.4 Equivalent viscous damping (*EVD*)

Wijesundara (Wijesundara *et al*. 2011) determined EVD for concentrically braced frames as a function of non-dimensional slenderness ratio, $\bar{\lambda}$, and the ductility, μ, as shown in the following equations

$$\xi = 0.03 + \left(0.23 - \frac{\bar{\lambda}}{15}\right)(\mu - 1) \qquad \mu \leq 2 \tag{12}$$

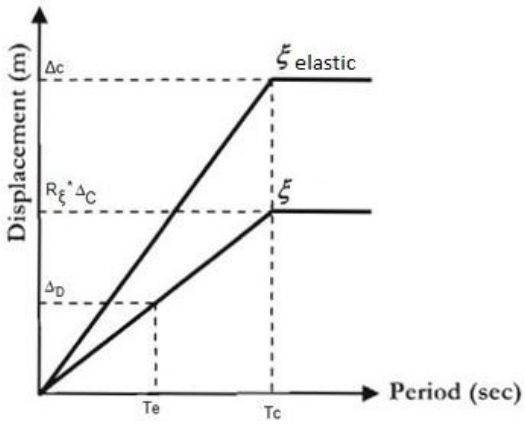

Fig. 1 Displacement response spectrum

$$\xi = 0.03 + \left(0.23 - \frac{\bar{\lambda}}{15}\right) \qquad \mu \geq 2 \tag{13}$$

This EVD model was verified using shake table tests and large range of NLTHA on single storey CBFs by Goggins and Salawdeh (2012).

2.5 Effective period

The effective period at the design displacement, T_e, can be read from the displacement spectrum, which is multiplied by a reduction factor giving the spectrum at the design damping level, as shown in Fig. 1.

Pennucci *et al*. (2011) studied displacement reduction factors for the design of medium and long-period structures. They suggested that if an existing EVD expression is used for design, it is important that it is used together with the damping reduction relationship that was used to develop the EVD expression itself from specific records. This is the reason that Priestley *et al*. (2007) have been advocating the use of the old EC8 (CEN 1998) damping reduction expression for DDBD for quite some time, even though it was known that the current EC8 (CEN 2004b) damping reduction expressions can better represent the effects of elastic damping on real ground motion spectra.

The reduction factor used in this work is the one used in 1998 edition of EC8 (CEN 1998), as the DDBD methodology was carried out using this expression and it was used to develop the EVD models by Wijesundara (2009), as shown in Eq. (14)

$$R_\xi = \left(\frac{0.07}{(0.02 + \xi)}\right)^{0.5} \tag{14}$$

where ξ is the equivalent viscous damping obtained from Eq. (12) or (13).

2.6 Effective stiffness of substitute structure

With the effective period established, the effective stiffness, K_e, is determined as

$$K_e = \frac{4\pi^2 m_e}{T_e^2} \tag{15}$$

where m_e is the mass calculated in Eq. (7) and T_e is the effective period.

2.7 Design base shear force

The base shear, V_{base}, is then obtained by multiplying the effective stiffness, K_e, by the design displacement, Δ_d, as the following equation

$$V_{base} = K_e \Delta_D \tag{16}$$

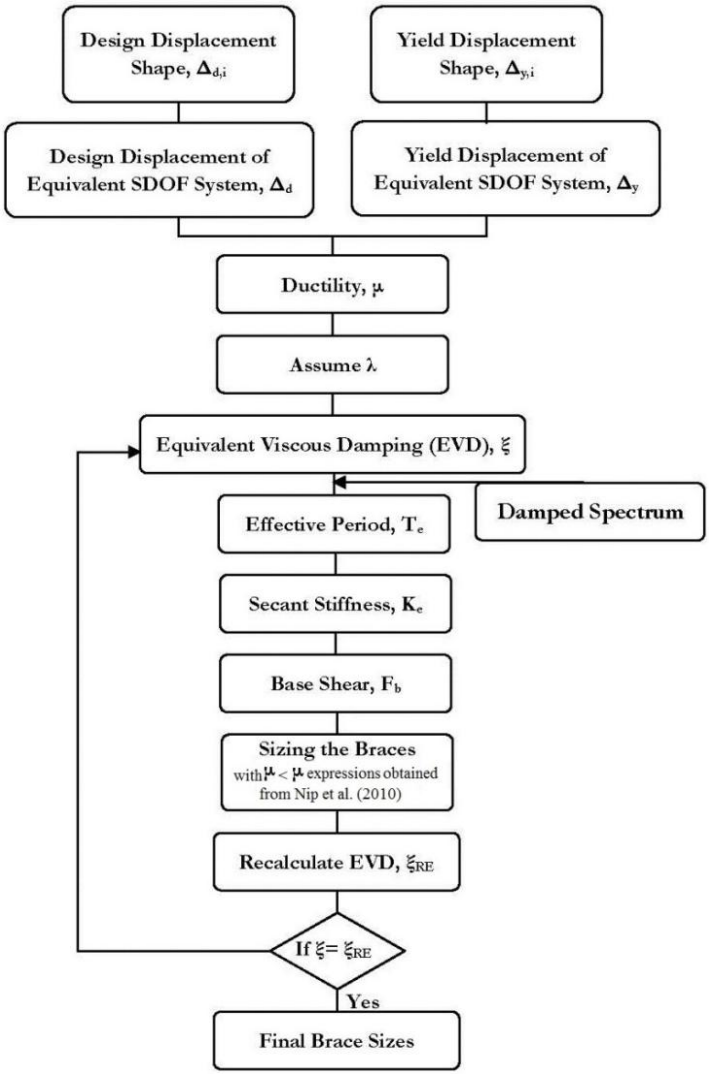

Fig. 2 Flow chart of the DDBD procedure for CBFs (adapted from Wijesundara (2011))

In the DDBD approach, it is recommended that the design base shear be increased to account for the reduction in effective lateral stiffness due to *P*-delta effects (Priestley *et al*. 2007). The increase in the lateral force required to account for *P*-Δ effects in steel structures can be estimated as

$$F_{P-\Delta} = \frac{m_e g}{H_e} \Delta_D \tag{17}$$

where g is acceleration due to gravity and H_e is the effective height of the SDOF system. Thus, the new base shear can be found by

$$V_{base} = K_e \Delta_D + \frac{m_e \mathrm{g}}{\mathrm{H_e}} \Delta_D \tag{18}$$

As suggested by Priestley *et al*. (2007), and in order to take into account the higher modes effect, 10% of the base shear force is allocated for to the roof level and the remaining 90% of the base shear force is distributed to all floor levels, including the roof, in proportion to the product of mass and displacement, as the follows

$$F_i = F_t + 0.9 V_{base} \frac{m_i \Delta_i}{\sum m_i \Delta_i} \tag{19}$$

where $F_t = 0.1 V_{base}$ at roof level and $F_t = 0$ at all other levels, V_{base} is the base shear, m_i and Δ_i are the mass and design displacement of the i^{th} floor, respectively.

A flow chart of the DDBD procedure for CBFs is shown in Fig. 2.

3. Case studies for DDBD for CBFs

Two case studies of 4-storey and 12-storey buildings are designed to investigate the DDBD for CBFs. The buildings' dimensions are 32 × 32 m in plan consisting of two CBFs in each direction as the lateral resistant frames. These buildings are symmetric in plan and elevation with a uniform storey height of 3 m. For simplicity, stiffness and strength contributions of the interior partitions and the exterior cladding are ignored and the accidental torsion is neglected. Plan view and elevation for the 4-storey structure are shown in Fig. 3. Columns are assumed to be continuous along the height and pinned at the base. The connections between columns and beams are assumed to be pinned and the lateral forces are assumed to be resisted by the braces on the 4m bays represented by the dashed lines.

Bracing end conditions are considered to be pinned in both ends. Characteristic dead and imposed loads of 8.1KPa and 3KPa, respectively, were selected using provisions of Eurocode 1 (CEN 2004a). Seismic loads were taken as the summation of the unfactored dead load and a reduced live load (seismic load = $G_k + 0.3 * Q_k = 8.1 + 0.3 * 3 = 9$ KPa, where G_k is the characteristic dead load and Q_k is the characteristic imposed load). Grade S355 steel with nominal yield strength of 355 N/mm^2 was chosen for all elements. Eurocode 8 (1) type 1 elastic response spectrum for soil type C and peak ground acceleration (PGA) of 0.3 g was chosen. Design storey drifts of 2.5% were selected to control damage of non-structural elements. To design the building, first the substitute structure displacement, Δ_D, effective mass, m_e, effective height, H_e, and ductility, μ, are

found. These were found to be 0.225 m, 1536 tonnes, 9 m and 5.22, respectively, as determined from Eqs. (6), (7), (8) and (9), respectively. The necessary calculations are summarised in Table 1.

To obtain the damping level, the equivalent viscous damping (EVD) equations suggested by Wijesundara (2009) are used, which are a function of ductility, μ, and non-dimensional slenderness ratio, $\bar{\lambda}$, as shown in Eqs. (12) and (13). Because the slenderness ratio is unknown at this stage of design an initial assumption of slenderness ratio is assumed to get the EVD. Then, the initial design of braces is carried out. A number of trials should be performed in which new shear forces and brace member sizes are found. These trials stop when the same brace sizes are found to be adequate for the two consecutive trial designs, as will be explained in the following. A slenderness ratio, $\bar{\lambda}$, is first assumed as 1.3 giving a damping ratio of 17.3% by employing the Eq. (13) from Wijesundara (Wijesundara 2009, Wijesundara *et al*. 2009).

Following the EC8 (CEN 2004b) recommendation for the relationship between damping and displacement reduction, the reduction factor to be applied to the 5% displacement spectrum to get the 17.3% displacement spectrum is found to be 0.602 using Eq. (14).

The displacement spectra for the design example are shown in Fig. 4, from which the effective period, T_e, corresponding to the design displacement, Δ_D, can be read and found to be 2.91 seconds.

By knowing m_e and T_e the effective stiffness is found 7171 kN/m using Eq. (15) and the base shear, V_{base}, is found as 1990.3 kN from Eq. (18).

Table 1 Calculations for design displacements, effective height and yield displacement

Level	Height (m)	Mass, m_i (ton)/fr	δ_i	Δ_{id}	$m_i\Delta_{id}$	$m_i\Delta_{id}^2$	$m_i\Delta_{id}H_i$	Δ_{iy}	$m_i\Delta_{iy}$	$m_i\Delta_{iy}^2$
4	12	460.8	1.00	0.30	138.24	41.47	1658.88	0.06	26.49	1.52
3	9	460.8	0.75	0.23	103.68	23.33	933.12	0.04	19.86	0.86
2	6	460.8	0.50	0.15	69.12	10.37	414.72	0.03	13.24	0.38
1	3	460.8	0.25	0.08	34.56	2.59	103.68	0.01	6.62	0.10
Sum		1843.2			345.60	77.76	3110.40		66.21	2.85

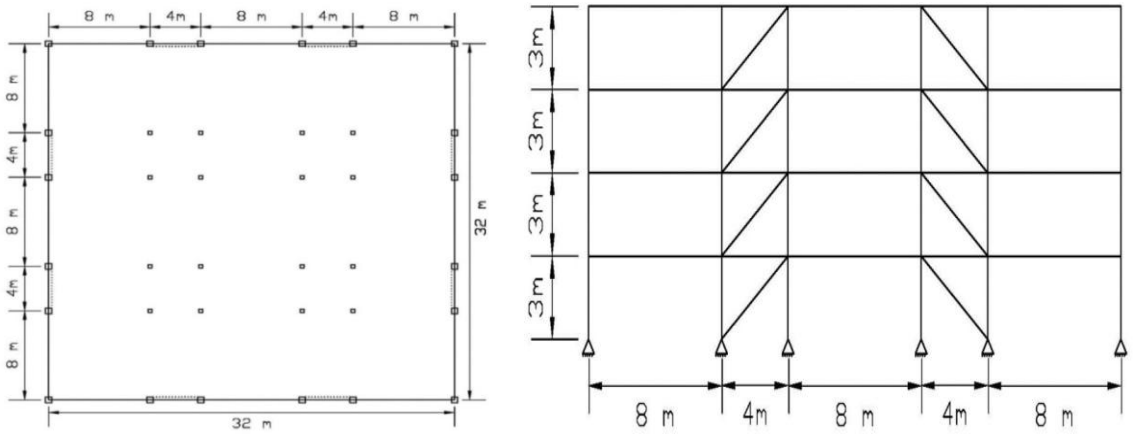

(a) (b)

Fig. 3 Four storey CBF case study (a) Plan view; (b) Elevation

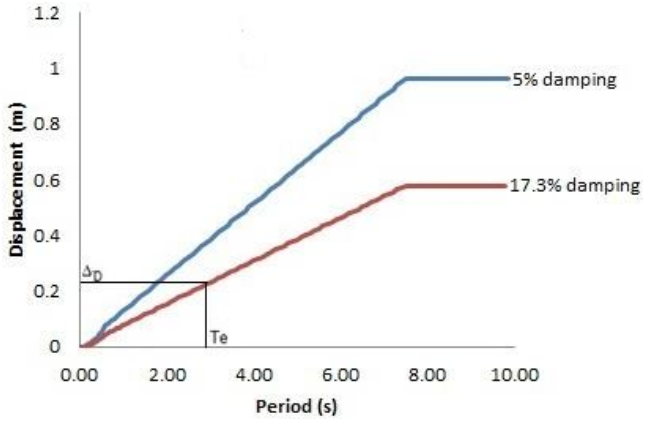

Fig. 4 Displacement response spectra for the 5% and 17.3% damping

3.1 Braces design

The base shear is distributed to the floor levels using Eq. (19) as shown in Table 2 for the initial calculations (i.e., iteration step n = 1). Storey shear forces, $V_{i,n}$ are found by summing the floor forces above the storey considered. Assuming only tension diagonal bracings resist the shear as suggested by EC8 (CEN 2004b), the axial force in the brace, $N_{Ed,i,n}$, is found by dividing the floor shear, $V_{i,n}$, by cosine of the angle of the brace with the horizontal, α. The brace area, $A_{b,n}$, is found by dividing the axial force in the brace, $N_{Ed,i,n}$, by the yield strength, f_y. All braces are chosen to be class 1 with a slenderness ratio $\bar{\lambda} \leq 2$, as suggested by EC8 (CEN 2004b), where $\bar{\lambda}$ is found by

$$\bar{\lambda} = \frac{L_{cr}}{i} \frac{1}{\lambda_1} \tag{20}$$

where L_{cr} is the length of the brace, i is radius of gyration and $\lambda_1 = 93.9\varepsilon$, where $\varepsilon = \sqrt{235/f_y}$. Note that Class 1 sections are defined as those that adhere to the limit $c/t \leq 33\varepsilon$, where c is width or depth of a part of the cross section ($c = h$ (or b) $- 2t - 2r$, where h is the height of the brace section, b is the width of the brace section, t is the thickness of the brace wall and r is the radius of root fillet), as described in EC3 (CEN 2005). A check for the brace overstrength, Ω, is carried out as the following

$$\Omega_{i,n} = \frac{N_{pl,Rd,i,n}}{N_{Ed,i,n}} \tag{21}$$

where $N_{pl,Rd,i,,n}$ is the design resistance of diagonal i and $N_{Ed,i,n}$ is the design demand value of the axial force in the same diagonal i in the seismic design situation. This check is carried out assuring that it satisfies the EC8 (CEN 2004b) requirements that the maximum brace overstrength does not differ from the minimum value by more than 25% in order to satisfy the homogeneous dissipative behaviour of the diagonals, as shown in Table 3. At this stage of design, the slenderness ratio and ductility are found for all the braces. So, the equivalent viscous damping can be found for every floor level using Eq. (13), as the real slenderness ratio values are found and the ductility, μ, is more than two. The new calculated equivalent viscous damping values, $\xi_{i,n+1}$, for every floor from

Table 2 Initial calculation of forces, shear and the design of brace elements

Level i	$F_{i,n}$ (kN)	$V_{i,n}$ (kN)	$N_{Ed,i,n}$ (kN)	Proposed area, $A_{b,n}$ (cm^2)	Section size	c/t	Class	i (cm)	$\bar{\lambda}_n$
4	916	916	1144	32.24	100×100×10	7	1	3.64	1.80
3	537	1453	1816	51.16	120×120×12.5	6.6	1	4.34	1.51
2	358	1811	2264	63.77	150×150×12.5	9	1	5.57	1.17
1	179	1990	2488	70.08	160×160×12.5	9.8	1	5.98	1.09
Sum	1990								

Table 3 Calculation of overstrength factor and the new equivalent viscous damping

Level, i	Real $A_{b,n}$ (cm^2)	$N_{pl,i,n}$ (kN)	$\Omega_{i,n}$	$\xi_{i,n+1}$	$V_{i,n}$*$\Delta_{D,i}$	$V_{i,n}$*$\Delta_{D,i}$*$\xi_{i,n+1}$
4	34.9	1239	1.08	0.14	274.66	38.49
3	52.1	1850	1.02	0.16	326.91	52.13
2	67.1	2382	1.05	0.18	271.68	49.36
1	72.1	2559	1.03	0.19	149.27	27.92
Sum					1022.52	167.90

iteration step n, are shown in Table 3. The equivalent viscous damping in iteration step n can be found by using the following equation

$$\xi_{n+1} = \frac{\sum V_{i,n}\Delta_{D,i}\xi_{i,n+1}}{\sum V_{i,n}\Delta_{D,i}} = \frac{167.90}{1022.52} = 0.1642 \tag{22}$$

The revised equivalent viscous damping is 5.4% less than the trial one found by using the assumed slenderness ratio. Thus, the above procedure is carried out again using the new equivalent viscous damping to ensure adequate braces are determined. The trials are finished when the same brace sizes are found to be adequate in two sequential trials.

The braces were chosen in this example after the second trial (i.e., n = 2), which are shown in Table 4. All braces satisfied the EC8 (CEN 2004b) requirements to be Class 1 with a slenderness ratio $\bar{\lambda} \leq 2$. Brace members were chosen carefully to represent the design values as close as possible, as the purpose of this design is to verify the design methodology, where the maximum brace overstrength factor, Ω_i, was 7%, as seen in Table 4.

Table 4 Final trial results of designing the braces

Level i	$F_{i,n}$ (kN)	$V_{i,n}$ (kN)	$N_{Ed,i,n}$ (kN)	Proposed $A_{b,n}$ (cm^2)	Section size	Real $A_{b,n}$ (cm^2)	$N_{pl,i,n}$ (kN)	$\Omega_{i,n}$	$\bar{\lambda}_{i,n}$
4	922	922	1153	32.48	100×100×10	34.9	1239	1.07	1.80
3	541	1464	1830	51.54	150×150×10	54.9	1949	1.07	1.15
2	361	1825	2281	64.25	150×150×12.5	67.1	2382	1.04	1.17
1	180	2005	2507	70.61	160×160×12.5	72.1	2560	1.02	1.09
Sum	2005								

3.2 Columns and Beams capacity design

Columns and beams are capacity designed to behave elastically by the following combination from EC8 (CEN 2004b), ensuring that dissipative behaviour is provided primarily by the braces. Thus, the following equations are employed in the design of columns and beams from EC8 (CEN 2004b).

$$N_{pl,Rd} \geq N_{Ed,G} + 1.1\gamma_{ov}\Omega N_{Ed,E} \tag{23}$$

$$M_{pl,Rd} \geq M_{Ed,G} + 1.1\gamma_{ov}\Omega M_{Ed,E} \tag{24}$$

$$V_{pl,Rd} \geq V_{Ed,G} + 1.1\gamma_{ov}\Omega V_{Ed,E} \tag{25}$$

where $N_{pl,Rd}$, $M_{pl,Rd}$ $V_{pl,Rd}$ are the design buckling resistance, bending moment capacity and shear resistance, respectively, of the beam or the column in accordance with EC3 (CEN 2005), taking into account the interaction of the buckling resistance with the bending moment. $N_{Ed,G}$, $M_{Ed,G}$ and $V_{Ed,G}$ is the axial force, bending moment and shear, respectively, in the beam or in the column due to the non-seismic actions included in the combination of actions for the seismic design situation. $N_{Ed,E}$, $M_{Ed,E}$ and $V_{Ed,E}$ are the axial force, bending moment and shear, respectively, in the beam or in the column due to the design seismic action. γ_{ov} is the overstrength factor taken as 1.25, while Ω is the brace overstrength taken as the minimum of Ω_i found in Eq. (21).

3.3 12-storey CBF case study

For the 12-storey building the same procedure is followed and a summary of the estimated final brace element sizes is given in Table 5.

Table 5 Structural member sizes and properties for the 12-storey building estimated using DDBD

Level	Braces				
	Section size	$A_{b,i,n}$ (cm^2)	$\bar{\lambda}_{i,n}$	$N_{pl,i,n}$ (kN)	$\Omega_{i,n}$
12	120×120×6.3	28.2	1.42	1001	1.22
11	120×120×10	42.9	1.47	15223	1.21
10	120×120×12.5	52.1	1.51	1850	1.11
9	140×140×12.5	62.1	1.27	2205	1.09
8	160×160×12.5	72.1	1.09	2560	1.08
7	180×180×12.5	82.1	0.96	2915	1.09
6	180×180×14.2	92	0.97	3266	1.11
5	180×180×16	102	0.99	3621	1.14
4	180×180×16	102	0.99	3621	1.08
3	200×200×16	115	0.88	4083	1.17
2	200×200×16	115	0.88	4083	1.13
1	200×200×16	115	0.88	4083	1.12

4. Verification of the DDBD procedure

In order to verify the performance of the DDBD method used to design the CBF case study structures, non-linear time history analyses (NLTHA) are carried out with time histories having displacement spectra that match the design spectrum used in the DDBD application. The computer program used for the verification is OPENSEES (McKenna *et al*. 2000), which is an object-oriented, open source software that allows users to create finite element applications for simulating the response of structural and geotechnical systems subjected to earthquakes.

4.1 Numerical model

Two-dimensional numerical models are employed, in which columns and beams are modelled to behave elastically. The connections between columns and beams, as well as between beams and braces, are assigned as pinned connections. Columns are assumed to be continuous along the height and pinned at the base. Braces are modelled as nonlinear beam-column element with distributed plasticity, where the cross section of the brace is divided into fibres along the perimeter and across the thickness. Three fibres are employed across the thickness and a minimum of $2(b + h)/3$ fibres around the perimeter of the cross section, where b and h are the width and the height of the cross section in mm. Thus, in total a minimum of 180 fibres are used in the cross section. This distribution of fibres gives optimum computational effort and accuracy as found in Salawdeh and Goggins (2013). The inelastic beam-column element is derived by small deformation theory, which is used for computation of local stresses and strains along the element. In accordance to the corotational theory described by Filippou and Fenves (2004), nonlinear geometry under large displacements is accounted for during transformation of the element forces and deformations to the global reference system. By using the corotational theory the moderate to large deformation effects of inelastic buckling of the concentric brace can be presented (small strains and large displacements). As a result of using this approach, the brace is suggested to be divided into a minimum of two elements using ten Gauss–Lobatto integration points per element (Salawdeh and Goggins 2013). An initial camber of 1% of the length of the brace is applied to the middle of the brace to account for the overall buckling. The initial camber is the main parameter that plays the major role for determining the first buckling load in the numerical model, but does not affect the general behaviour of the hysteretic response. Several researchers (Hu 2014, Nascimbene *et al*. 2012, Uriz *et al*. 2008, Wijesundara *et al*. 2009, 2014, Yoo *et al*. 2008) carried out comparisons between numerical and experimental models and suggested using different initial cambers, where a lower initial camber values are found for stockier specimens and larger initial camber values are found for more slender specimens. A low cyclic fatigue model with parameters calibrated by Salawdeh and Goggins (2013) is used to wrap the fibre based nonlinear beam column model in order to capture fracture in the braces. Uniaxial Giuffre-Menegotto-Pinto steel material model with isotropic strain hardening and monotonic envelop is used in this study with a value of strain hardening equal to 0.008. More information about the model of the brace element can be found in Salawdeh and Goggins (2013).

A solution algorithm of type Krylov–Newton is used. This solution algorithm tests convergence on the norm of the displacement increment vector with a tolerance of 1e-12 and a maximum number of iterations of 1000. The numerical integration method used to evaluate the dynamic response of the structure is Hilber-Hughes-Taylor (HHT) method, which is an extension to the Newmark method with constant Gamma equal to 0.5. The Rayleigh damping model is used, which

assumes that the damping matrix is proportional to the mass and stiffness matrices. Elastic damping of 3% was specified. A similar value was found from the physical tests and used in the DDBD methodology. The numerical model was verified using cyclic tests in braces (Salawdeh and Goggins 2013) and shake table tests for single storey CBF structures (Goggins and Salawdeh 2012).

4.2 Ground motions used in the study

Eight different accelerograms from four different earthquakes (2 components in orthogonal direction for each earthquake) taken from Pennucci *et al*. (2011) are employed in the NLTHA models to validate the DDBD procedure. They are shown in Table 6, which gives the ID used for the study, date of the earthquake, PEER ID, the magnitude, M and the epicentre distance, r. Time history accelerograms are scaled to get a displacement response spectrum that matches the soil type C design displacement spectrum with 5% damping from EC8 (CEN 2004b), which was used in the DDBD for the case studies. Response spectra for the scaled accelerograms are found using the programme SeismoSignal (2007) for the elastic response spectra with 5% damping, as shown in Fig. 5.

4.3 Comparison of results from NLTHA and DDBD

For the 4-storey and the 12-storey CBF structures, the maximum floor displacements, taking into account the higher modes effect, are found during nonlinear time-history analyses for the

Table 6 Properties of the first set ground motions

Earthquake	ID used	Date	PEER ID	Magnitude, *M*	Distance, *r* (km)
Northridge	EQ3a, EQ3b	Jan. 17, 1994	959	6.7	5
Imperial Valley	EQ4a, EQ4b	Oct. 15, 1979	169	6.5	34
Hector	EQ5a, EQ5b	Oct. 16, 1999	1762	7.13	48
Landers	EQ6a, EQ6b	Jun. 28, 1992	900	7.28	86

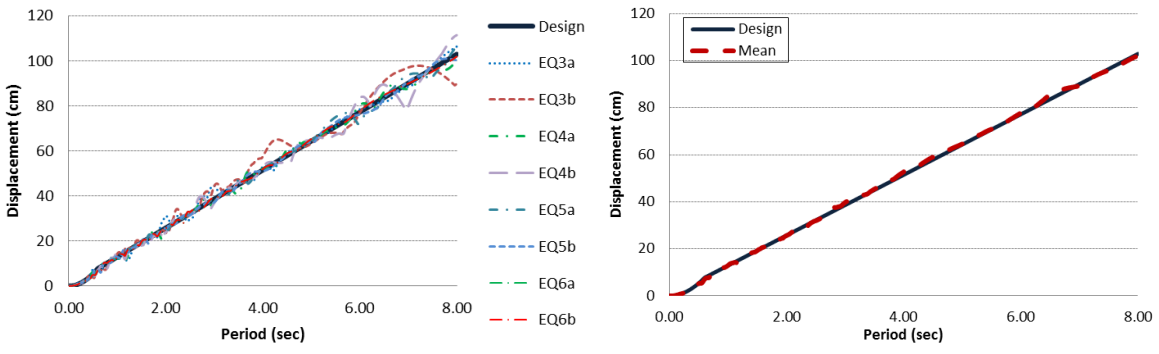

(a) (b)

Fig. 5 5% design spectrum compared to the scaled displacement spectra for (a) eight accelerograms used to verify the design procedure using NLTHA; (b) the average of eight accelerograms used to verify the design procedure using NLTHA

eight accelerograms. These are compared with the design displacement profiles obtained from the DDBD method, as shown in Fig. 6. Similarly, the average of the maximum recorded displacement during time-history analyses for the eight accelerograms and the design displacement profiles are shown in Fig. 7 for the 4-storey and the 12-storey buildings. It is apparent that the maximum displacements recorded from the time history analyses for the 4-storey and the 12-storey buildings are conservatively representing the design displacements assumed. One reason is that in the design it was assumed that the tension brace only resists the earthquakes. However, it is found that the compression brace also contributes to the lateral resistance in CBFs (Goggins 2004). Furthermore, 10% of the base shear was assigned to be resisted by top floor to account for the higher mode effects, which leads to stronger upper storeys. While trying to account for the compression brace in the design, it is found that in some storeys failure of one of the braces occurred causing soft storey. So it was decided to be safe and conservative and assume all the lateral forces are resisted by the tension braces only, which is also a requirement in EC8 (CEN 2004b).

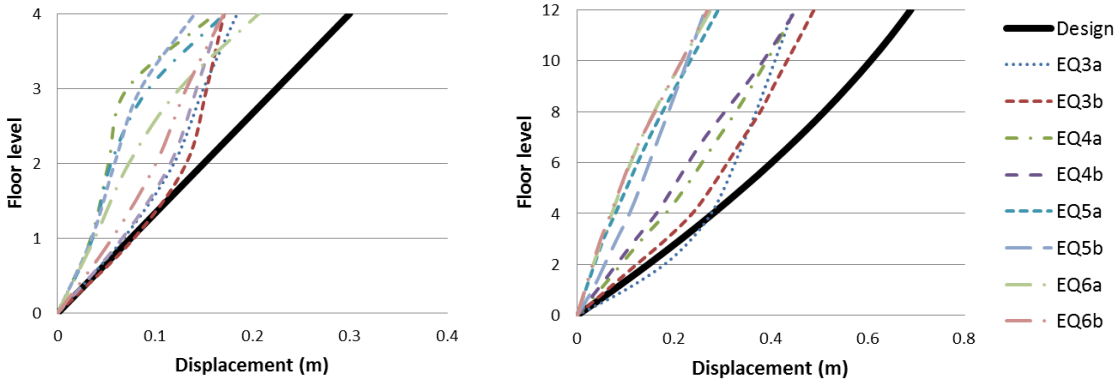

(a) (b)

Fig. 6 Maximum recorded displacements for eight spectrum compatible accelerograms compared with the design displacements for (a) a 4-storey CBF; and (b) a 12-storey CBF

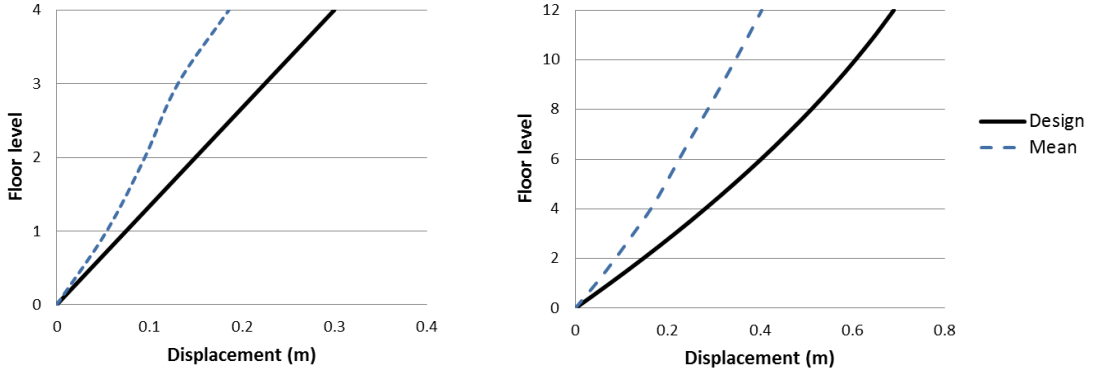

(a) (b)

Fig. 7 Average of the maximum recorded displacements for eight spectrum compatible accelerograms compared with the design displacements for the (a) 4-storey CBFs and (b) the 12-storey CBFs

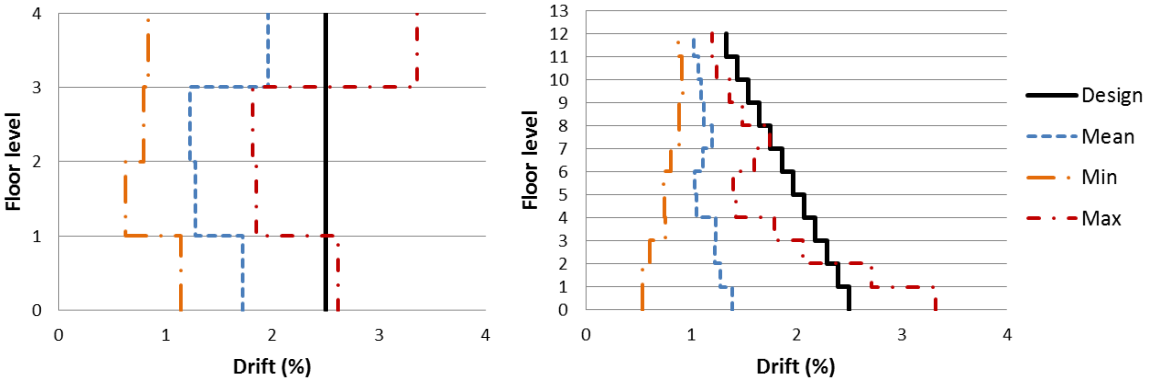

(a) (b)

Fig. 8 Average of the maximum recorded storey drifts for eight spectrum compatible accelerograms compared with the design storey drifts for the (a) 4-storey CBF; and the (b) 12-storey CBF

The average of the maximum storey drifts recorded during time-history analyses using the eight accelerograms compared with the linear displacement design drift profile assumed for the case studies are shown in Fig. 8 for the 4- and 12-storey buildings. It is found that the average of the maximum recorded storey drifts for the eight accelerograms for the 4- and 12-storey buildings are conservatively less than the design storey drift profile for the reasons mentioned earlier.

The maximum recorded ductility values are found during nonlinear time-history analyses for the eight accelerograms for the 4-storey and the 12-storey buildings. These are compared with the design ductility values obtained from the DDBD method, as shown in Fig. 9. It is found that the maximum ductility observed from the time history analyses for the 4-storey and the 12-storey CBFs are in general less than the ductility used in the design. The main reason for this is that in the design, the lateral forces in the structure induced by the earthquakes were assumed to be resisted by the tension brace members only. However, as noted later the base shear is resisted by braces in both tension and compression, albeit the contribution of the compression member is significantly less than that of the tension member.

The averages of the maximum recorded ductility during time-history analyses for the eight accelerograms are shown in Fig. 10 for the 4-storey and the 12-storey buildings. These are compared to the design ductility obtained from the DDBD method, ductility expressions established by Nip *et al*. (2010a, b) for hot-rolled and cold-formed carbon steel shown in Eqs. (26) and (27), respectively, and a ductility expression established by Tremblay (2002) shown in Eq. (28). It is apparent that the average of the maximum ductility values recorded from the time history analyses for the 4-storey and the 12-storey buildings are lower than the design ductility from the DDBD method and ductility expressions established by Nip *et al*. (2010b) and Tremblay (2002).

Hot-rolled steel:
$$\mu_f = 3.69 + 6.97\bar{\lambda} - 0.05\left(\frac{b}{t\varepsilon}\right) - 0.19\left(\bar{\lambda}\right)\left(\frac{b}{t\varepsilon}\right) \tag{26}$$

Cold-formed steel:
$$\mu_f = 6.45 + 2.28\bar{\lambda} - 0.11\left(\frac{b}{t\varepsilon}\right) - 0.06\left(\bar{\lambda}\right)\left(\frac{b}{t\varepsilon}\right) \tag{27}$$

$$\mu_f = 2.4 + 8.3\bar{\lambda} \tag{28}$$

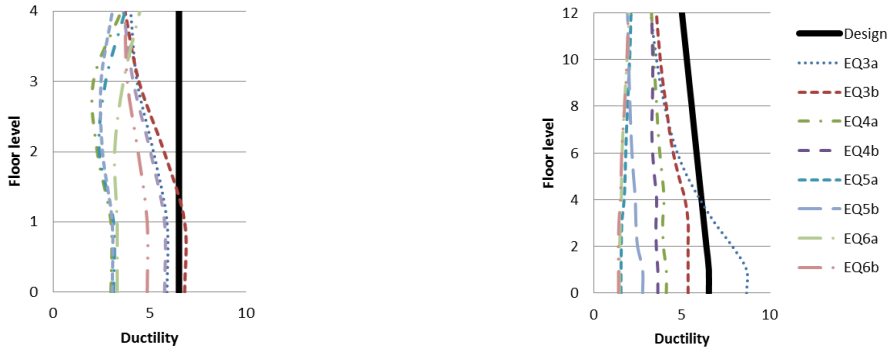

(a) (b)

Fig. 9 Maximum recorded ductility for eight spectrum compatible accelerograms compared with the design ductility for (a) 4-storey CBF; and (b) 12-storey CBF

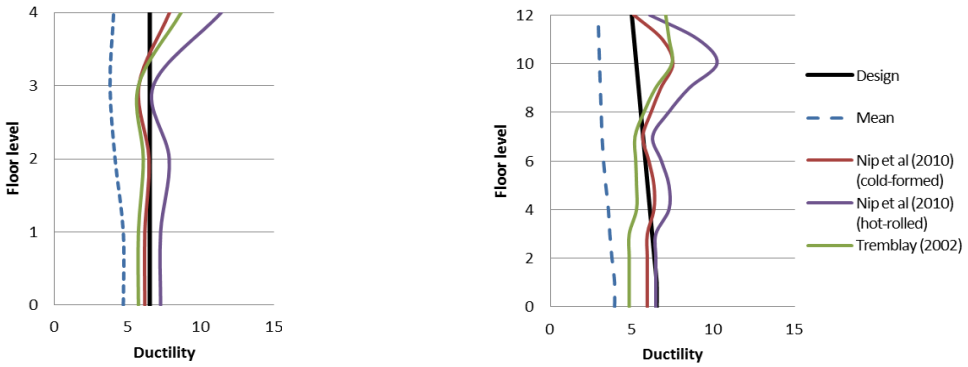

(a) (b)

Fig. 10 Average of the maximum recorded ductility for eight spectrum compatible accelerograms compared to the design ductility, ductility expressions of Nip *et al*. (2010b) for cold-formed and hot-rolled carbon steel and ductility expression of Tremblay (2002) for (a) 4-storey CBF; and (b) 12-storey CBF

As described in Section 3.1, the design base shear was distributed to the floors and assumed to be resisted by tension braces only in the DDBD of the case study buildings. Compression members were assumed not to resist any load, as suggested by EC8 (CEN 2004b). The design shear force from the DDBD procedure outlined in Section 3 and the shear force resisted by every brace at the instance when maximum displacement occurs in the NLTHA for the 4-storey and 12-storey CBF structures are shown from Fig. 11 and 12, respectively. As discussed previously, the compression member braces also resisted lateral forces and, thus, the predicted displacement and drift profiles were conservative as the system had a higher lateral resistance than assumed in the design. The mean of the shear forces resisted by both of the braces at the maximum displacement demand during the eight earthquakes are compared to the design shear forces in Fig. 13 for the 4-storey and 12-storey CBF.

Braces with low slenderness ratio are found to have more compressive strength capacity compared to slender braces, as observed in the lower floor shears that have stocky members. It is

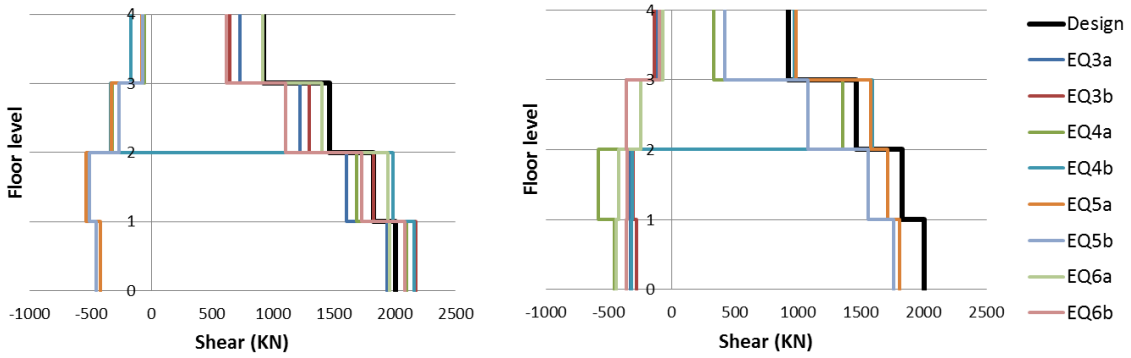

(a) (b)

Fig. 11 4-storey CBF shear force design values compared to shear at the maximum displacement from NLTHA using eight earthquakes resisted by (a) first brace; and (b) second brace. Negative sign represents compression resistance and positive sign represents tension

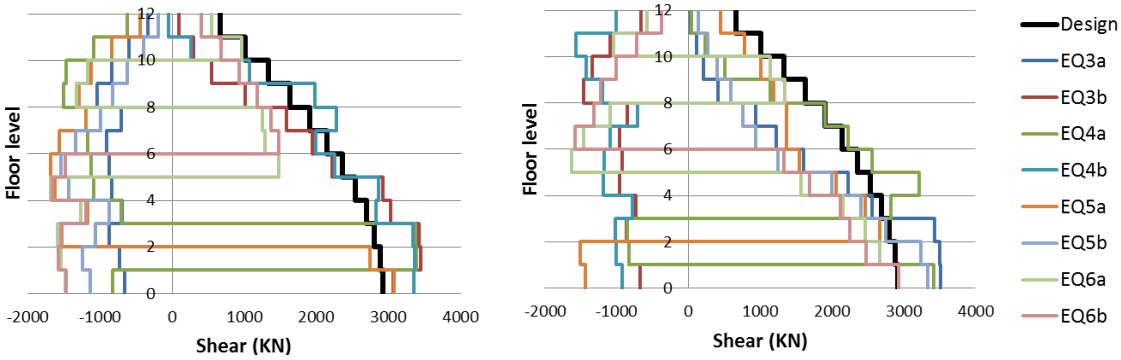

(a) (b)

Fig. 12 12-storey CBF shear force design values compared to shear at the maximum displacement from NLTHA using eight earthquakes resisted by (a) first brace; and (b) second brace. Negative sign represents compression resistance and positive sign represents tension

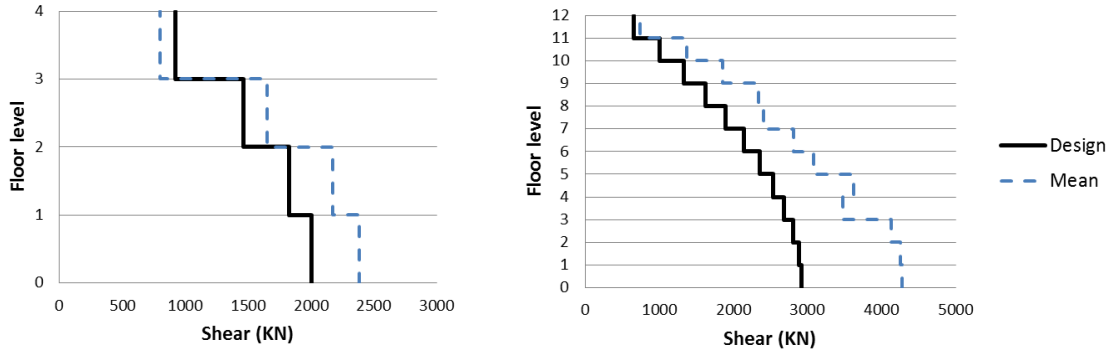

(a) (b)

Fig. 13 Average total shear forces resisted by both compression and tension braces from NLTHA using eight earthquakes compared to the design shear forces of (a) 4-storey; CBF (b) 12-storey CBF

noted that compression shear resisted at the maximum displacement was less than the shear at the first buckling load due to residual deformation and Bauschinger effect. Residual stresses may as well influence the behaviour of the structure (Besevic 2012). As discussed previously, applying a percentage between 10% and 30% of the lateral force to be resisted by compression brace members led to fracture occurring in most of the slender braces located at the top floors in the NLTHA. Thus, it was decided to adopt the design philosophy that lateral forces are resisted only by tension bracing members and the contribution to the lateral resistance of the system by the compression member is ignored.

5. Design of CBFs according to FBD

In this section an investigation of the seismic performance of CBFs is carried out when designed according to the FBD approach outlined in EC8 (CEN 2004b). To do this, both of the 4- and 12-storey case studies of the CBF buildings detailed in Section 3 are re-designed using the FBD approach, and then the performance is gauged with NLTHA and compared with the DDBD solutions. The details of 4-storey building design procedure will be detailed in the following sections.

5.1 Design response spectrum and seismic forces

EC8 (CEN 2004b) type 1 elastic response spectrum for soil type C and peak ground acceleration (PGA) of 0.3 g are chosen. The importance factor γ_I for ordinary building is taken as 1. Therefore, the design ground acceleration on type C ground ($a_q = \gamma_I \, a_{qR}$) is 0.3 g. The fundamental period of vibration of the building for lateral motion in the direction considered, T_1, can be found by the following

$$T_1 = C_t H^{3/4} \tag{29}$$

where C_t is 0.050 for CBFs and H is the height of the building in metres from the foundation. The height of the 4-storey building is 12 m, and, thus, T_1 is equal to 0.32 seconds.

To take into account the capacity of the structure to dissipate energy, FBD uses the design spectrum, S_d. This can be obtained by reducing the ordinates of the reference elastic spectrum, S_e, by means of a behaviour (reduction) factor, q, which allows for the ductility expected for the structural system. EC8 (1) specify a value of 4 for the behaviour factor, q, for diagonal CBFs. The values of the periods $T_B = 0.20$, $T_C = 0.6$, $T_D = 2.0$ and the soil factor $S = 1.15$ describing the shape of the elastic response spectrum for ground type C for type 1 are found from EC8 (CEN 2004b). As $T_B \leq T_1 \leq T_C$, then the ordinate of the design spectrum at period T_1 is as follows

$$S_d(T_1) = a_g * S * \frac{2.5}{q} = 0.3 * 9.81 * 1.15 * \frac{2.5}{4} = 2.12 \; m/s^2 \tag{30}$$

The seismic base shear, F_b, can be found by the following

$$F_b = S_d(T_1).m.\lambda \tag{31}$$

where m is the total mass of the building above the foundation or above the top of a rigid basement, which is computed as the addition of the gravity dead load and 0.3 of the gravity live load. Λ is the

Table 7 Storey forces and design shear for the 4-storey case study structure

Level, i	Height (m)	Mass, m_i (ton)/frame	$m_i z_i$ (ton.m)	F_i (kN)	V_i (kN)
4	12	460.8	5530	1326	1326
3	9	460.8	4147	994	2320
2	6	460.8	2765	663	2983
1	3	460.8	1382	331	3314
Sum		1843.2	13824	3314	

Table 8 Calculation of brace axial forces and the design of brace elements

Level	$N_{Ed,I}$ (kN)	Proposed area, A_b (cm^2)	Section size	$\bar{\lambda}$	Real A_b (cm^2)	$N_{pl,I}$ (kN)	Ω_i
4	1657	46.68	140×140×10	1.26	48.6	1725	1.04
3	2900	81.68	200×200×12	0.87	84.1	2986	1.03
2	3728	105.02	250×250×12	0.69	108	3834	1.03
1	4143	116.69	300×300×12	0.56	132	4686	1.13

correction factor, the value of which is equal to 0.85 if $T_1 < 2T_C$ and the building has more than two storeys, where T_C is the upper limit of the period of the constant spectral acceleration branch, or λ = 1.0 otherwise. The seismic base shear, F_b, for the case study using Eq. (31) is 3314 kN.

When the fundamental mode shape is approximated by horizontal displacements increasing linearly along the height, the horizontal forces, F_i, can be given at each storey I as follows

$$F_i = F_b \frac{m_i z_i}{\sum m_j z_j} \tag{32}$$

where z_i, z_j are the heights of the masses m_i, m_j above the level of application of the seismic action. Storey forces and design shear are shown in Table 7.

5.2 Design of braces

EC8 (CEN 2004b) assumes that storey shear at all floor levels are entirely resisted by axial forces in braces and only tension diagonal bracings resisting the shear forces. Thus, the axial force in the brace, $N_{Ed,I}$, is found by dividing the floor shear, $V_{i,n}$, by cosine of the angle of the brace with the horizontal, α. The brace area is found by dividing the axial force in the brace, $N_{Ed,I}$, by the yield strength, f_y, which is taken as 355 N/mm^2 in this case study. All braces are chosen to be Class 1 with a slenderness ratio $\bar{\lambda} \leq 2$, as suggested by EC8 (CEN 2004b), where slenderness ratio, $\bar{\lambda}$, is found by Eq. (20). A check for the brace overstrength, Ω, is carried out by Eq. (21). This check is carried out assuring that it satisfies the EC8 (CENR 2004b) requirements that the maximum brace overstrength does not differ from the minimum value by more than 25% in order to satisfy the homogeneous dissipative behaviour of the diagonals, as shown in Table 8.

5.3 Beams and columns design

Columns and beams are capacity designed to behave elastically ensuring that dissipative

Table 9 Column and beam designed sections from capacity design principles

Level, *i*	Columns	Beams
4	HD 320×127	HE 320 B
3	HD 400×237	HE320 M
2	HD 400×287	HE 340 M
1	HD 400×314	HE 400 M

Table 10 Calculations of elastic displacement, design displacement and drift

Level, *i*	d_e (m)	d_s (m)	Drift (%)
4	0.0302	0.1208	0.97
3	0.0229	0.0916	1.08
2	0.0148	0.0592	1.04
1	0.007	0.028	0.93

behaviour is provided primarily by the braces. This is achieved by following the combination from EC8 (CEN 2004b). Thus, equations from (23) to (25) are employed in the design of columns and beams from EC8 (CEN 2004b). The selected beams and columns for the 4-storey building are shown in Table 9.

5.4 Inter-storey drift limitation

EC8 (CEN 2004b) suggests that the displacements induced by the design seismic action shall be calculated on the basis of the elastic deformations of the structure by the following expression

$$d_s = q_d \, . d_e \tag{33}$$

where d_s is the displacement of a point of the structure induced by the design seismic action, q_d is the displacement behaviour factor assumed equal to q, and d_e is the elastic displacement of the same point of the structure. The elastic displacement is found using the software SAP2000 (2002). The design lateral displacement, d_s, is found from Eq. (33) and is shown in Table 10. From Table 10, it is found that the design drift is less than the maximum allowable drift assumed (2.5%). Therefore, the section sizes found using FBD are acceptable.

5.5 P-Δ effect

EC8 (CEN 2004b) suggests that *P*-Δ effects need not be taken into account if the following condition is fulfilled in all storeys

$$\theta = \frac{P_{tot}}{V_{tot}} \frac{d_r}{h} \leq 0.1 \tag{34}$$

where θ is the inter-storey drift sensitivity coefficient, P_{tot} is the total gravity load at and above the storey considered in the seismic design situation, d_r is the design inter-storey drift and evaluated as

Table 11 Calculation of the inter-storey drift sensitivity coefficient

Level, i	P_{tot}	V_{tot}	d_r	θ
4	460.80	1325.62	0.0292	0.003
3	921.60	2319.84	0.0324	0.004
2	1382.40	2982.65	0.0312	0.005
1	1843.20	3314.05	0.028	0.005

Table 12 Section sizes and slenderness ratios for the 12-storey CBF case study

Level, i	Braces design using FBD				
	Section size	$A_{b,\mathrm{I},n}$ (cm^2)	$\bar{\lambda}_{i,n}$	$N_{pl,\mathrm{I},n}$ (kN)	$\Omega_{i,n}$
12	200×200×8	54.4	0.84	1931	1.24
11	260×260×10	98.9	0.64	3511	1.17
10	260×260×12.5	122	0.65	4331	1.01
9	300×300×16	179	0.57	6355	1.16
8	450×250×16	211	0.64	7491	1.15
7	400×400×16	243	0.42	8627	1.16
6	400×400×16	243	0.42	8627	1.05
5	400×400×20	300	0.42	10650	1.20
4	400×400×20	300	0.42	10650	1.14
3	400×400×20	300	0.42	10650	1.09
2	400×400×20	300	0.42	10650	1.06
1	400×400×20	300	0.42	10650	1.05

the difference of the lateral displacements d_s at the top and bottom of the storey under consideration, V_{tot} is the total seismic storey shear and h is the inter-storey height.

EC8 (CEN 2004b) suggests that if $0.1 < \theta \leq 0.2$, the P-Δ effects may approximately be taken into account by multiplying the relevant seismic action effects by a factor equal to $1/(1-\theta)$. The maximum acceptable value of the coefficient θ is 0.3. Calculations of the inter-storey drift sensitivity coefficients, θ, are shown in Table 11 for each level of the building. It is found that θ is less than 0.1 for all storeys, so it is not necessary to take into account P-Δ effects. Brace section sizes, slenderness ratios, $\bar{\lambda}_{i,n}$, design resistance, $N_{pl,\mathrm{I},n}$ and brace overstrength factors, $\Omega_{i,n}$, of the braces for the 12-storey CBF structure found using FBD are shown in Table 12.

6. Comparison of FBD approach with DDBD and NLTHA

In this section a comparison is carried out between the 4- and 12-storey structure designed using the DDBD approach in Section 3 with that designed using the FBD approach in Section 5. Furthermore, the predicted performance of the structure designed using the FBD approach will be obtained using NLTHA and salient response parameters are discussed.

The NLTHA numerical model used to verify the DDBD procedure is used here to verify the FBD approach. Eight different accelerograms from four different earthquakes taken from Pennucci

et al. (2011) and shown in Table 6 are used in the NLTHA.

Time history accelerograms are scaled to get a displacement response spectrum that matches the soil type C design displacement spectrum with 5% damping from EC8 (CEN 2004b), which was used in the FBD approach for the case study. Response spectra for the scaled accelerograms are found using the SeismoSignal (2007) for the elastic response spectra with 5% damping, as shown in Fig. 5.

When comparing the 4- and 12-storey case study structures designed using both the DDBD and FBD approaches, it is found that the seismic base shear, F_b, from the FBD is larger than the base shear obtained from DDBD. This leads to the use of larger sections for the structure designed by FBD approach to resist the lateral forces. Because of that, the lateral displacements the structure endures in the FBD approach are less than the design lateral displacements used to design the

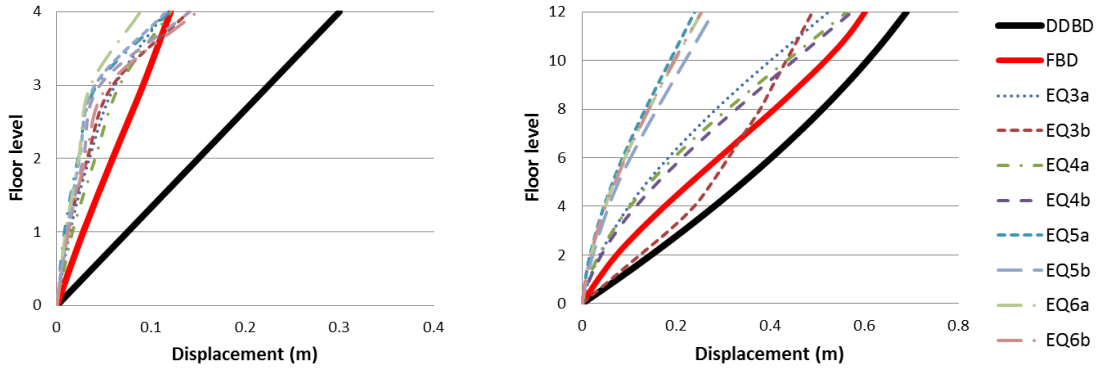

(a) (b)

Fig. 14 Maximum recorded displacements for eight spectrum compatible accelerograms compared with the design displacements used for the DDBD and the displacements obtained from FBD approach for (a) 4-storey CBFs; and (b) 12-storey CBF case study structures that were designed using FBD

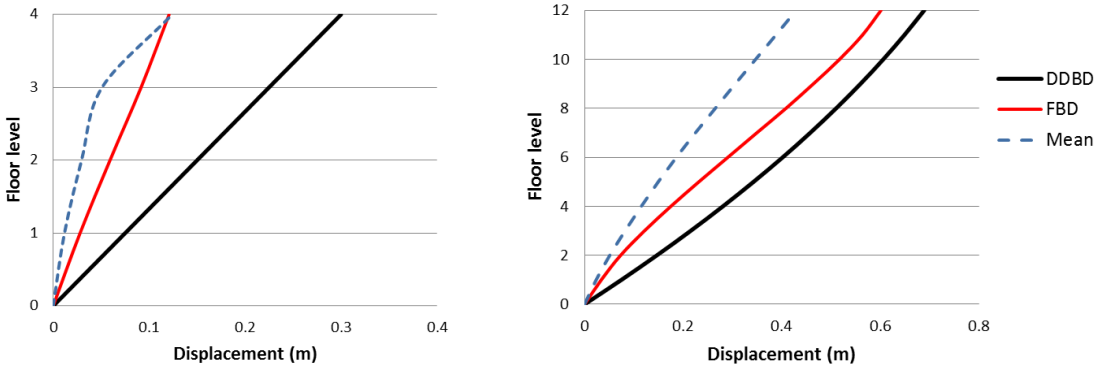

(a) (b)

Fig. 15 Average of the maximum recorded displacements for eight spectrum compatible accelerograms compared with the design displacements used for the DDBD and the displacements obtained from FBD approach for (a) 4-storey CBF; and (b) 12-storey CBF case study structures that were designed using FBD

structure in DDBD approach. Furthermore, the larger base shear forces experienced in the structure designed using the FBD approach will lead to higher demands on foundations.

The maximum floor displacements are found during NLTHA for the eight different accelerograms for the 4- and 12-storey case study structures that were designed using FBD. These are compared with the design displacement profile obtained from the FBD approach and the displacement profile used in DDBD, as shown in Fig. 14. Similarly, the average of the maximum recorded displacement during time-history analyses for the eight accelerograms, the design displacement profile from DDBD and the displacement profile obtained from FBD are shown in Fig. 15. It is apparent that the maximum displacements recorded from the time history analyses and from the FBD approach are less than the linear design displacements assumed for the DDBD procedure.

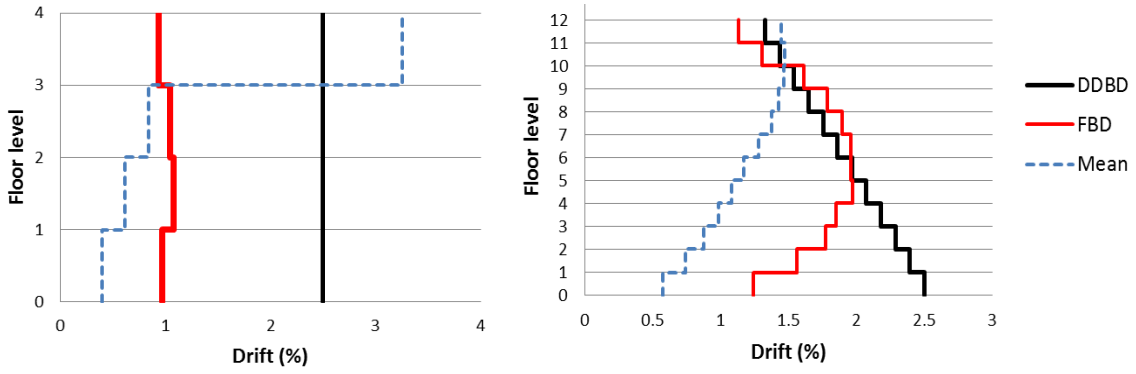

(a) (b)

Fig. 16 Average of the maximum recorded storey drifts for eight spectrum compatible accelerograms compared with the design storey drifts used for the DDBD and the drifts obtained from FBD approach for the (a) 4-storey CBF; and (b)) 12-storey CBF case study structures that were designed using FBD

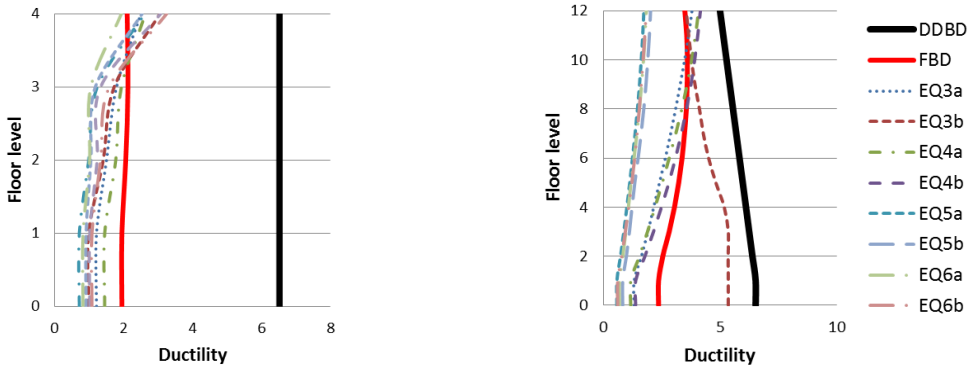

(a) (b)

Fig. 17 Maximum recorded ductility for eight spectrum compatible accelerograms compared with the design ductility from DDBD and FBD method for the (a) 4-storey CBFs; and (b) 12-storey CBFs case study structures that were designed using FBD

The average of the maximum recorded storey drifts for the eight accelerograms for the 4-storey and 12-storey buildings are less than the design storey drift profile obtained from FBD and used in DDBD for most of the storeys (Fig. 16). This is due to the design assumption that the tension brace member only is assumed to contribute to the lateral resistance of the system. On the other hand, the average maximum drift obtained from the NLTHA was more than the design drift for the top storey due to higher mode effects. Because of that and in order to take into account the higher modes effect, 10% of the base shear force should be allocated for to the roof level and the remaining 90% of the base shear force should be distributed to all floor levels including the roof in proportion to the product of mass and displacement, as suggested by Priestley *et al.* (2007) and shown in Eq. (19). This is the approach taken in the DDBD method used above.

The maximum recorded ductility values are found during nonlinear time-history analyses for

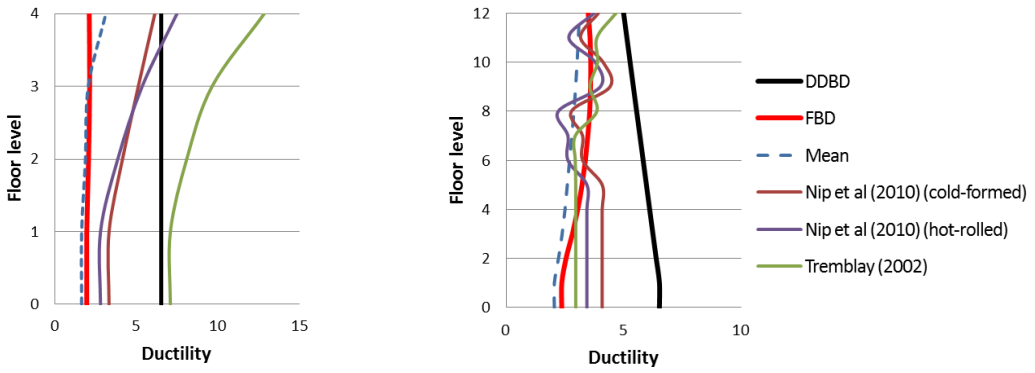

(a) (b)

Fig. 18 Average of the maximum recorded ductility for eight spectrum compatible accelerograms compared to the design ductility from DDBD and FBD approach, ductility expressions of Nip *et al.* (2010) for cold-formed and hot-rolled carbon steel and ductility expression of Tremblay (2002) for the (a) 4-storey CBFs; and (b) 12-storey CBFs case study structures that were designed using FBD

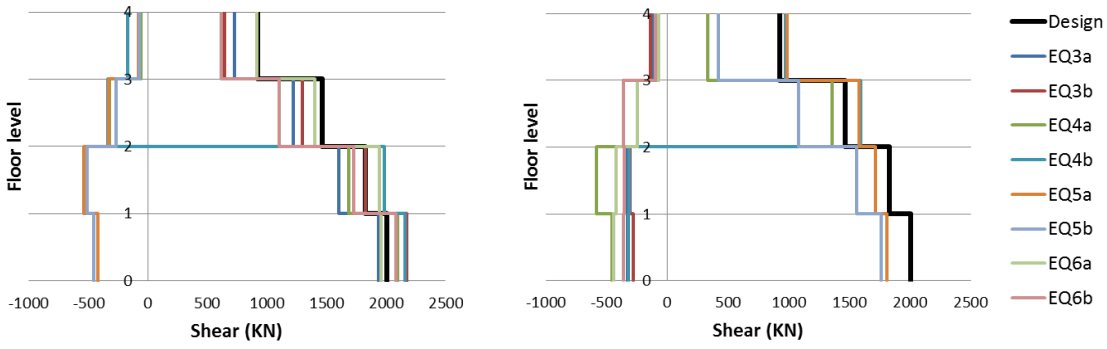

(a) (b)

Fig. 19 4-storey CBF shear force design values compared to shear at the maximum displacement from NLTHA using eight earthquakes resisted by (a) first brace; and (b) second brace case study structures that were designed using FBD. Negative sign represents compression resistance and positive sign represents tension

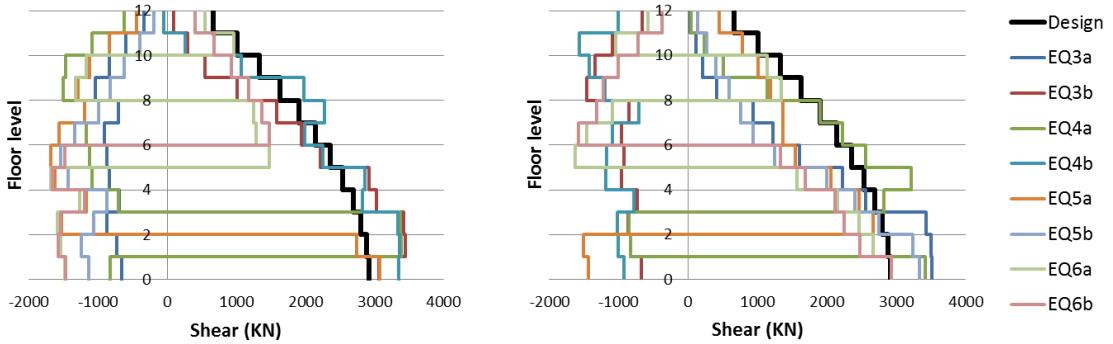

(a) (b)

Fig. 20 12-storey CBF shear force design values compared to shear at the maximum displacement from NLTHA using eight earthquakes resisted by (a) first brace; and (b) second brace for case study structures that were designed using FBD. Negative sign represents compression resistance and positive sign represents tension

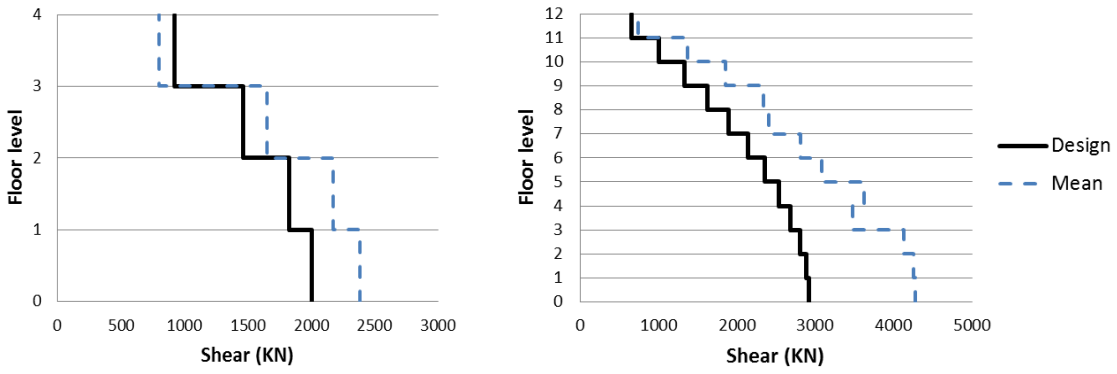

(a) (b)

Fig. 21 Average total shear forces resisted by both compression and tension braces from NLTHA using eight earthquakes compared to the design shear forces obtained from FBD approach for the (a) 4-storey CBF; and (b) 12-storey CBF case study structures that were designed using FBD

the eight accelerograms for the case study buildings. These are compared with the design ductility values obtained from the DDBD and FBD method, as shown in Fig. 17. It is found that the maximum ductility demand estimated from the time history analyses for the case study is in general very close to the ductility found from FBD approach and less than the ductility used in the DDBD. This is due to the larger section sizes required in the structure designed using the FBD approach.

The averages of the maximum recorded ductility during time-history analyses for the eight accelerograms are shown in Fig. 18 for the case study buildings. These are compared to the design ductility obtained from the FBD and the DDBD methods, as well as ductility expressions established by Nip *et al.* (2010b) shown in Eqs. (26) and (27), respectively, and ductility expression established by Tremblay (2002) shown in Eq. (28). It is apparent that the average of the maximum ductility values recorded from the time history analyses for the case study building are

close to the design ductility obtained from FBD and lower than the design ductility from the DDBD method and ductility expressions established by Nip *et al*. (2010b) and Tremblay (2002).

The design base shear was distributed to the floors by Eq. (32) and assumed to be resisted by tension braces only in the FBD case study buildings. Compression members were assumed not to resist any load as suggested by EC8 (CEN 2004b). The design shear force from the FBD procedure and the shear force resisted by every brace at the instance when maximum displacement occurs in the NLTHA for the 4-storey CBF structure are shown in Figs. 19 and 20. As discussed previously in the DDBD approach, the compression member braces also resisting lateral forces. The mean of the shear forces resisted by both of the braces at the maximum displacement demand during the eight accelerograms are compared to the design shear forces in Fig. 21.

7. Conclusions

A DDBD methodology for steel multi-storey CBFs has been validated. A linear displacement profile shape was found to give conservatively adequate approximation for the displaced shape of multi-storey CBFs. In this design methodology, columns and beams were capacity designed to behave elastically and all the lateral forces were considered to be resisted by tension brace members only. Columns were chosen to be continuous along the building height and pinned at the base. The connections between columns and beams were considered to be pinned. Furthermore, bracing end conditions were considered to be pinned in both ends.

Two case studies of 4-storey and 12-storey CBFs were carried out to verify the DDBD procedure. NLTHA, which was advanced using shake table tests for real one-storey-one-bay CBFs, was used to check the validity of the method on the case studies using eight different accelerograms with displacement spectra matching the design displacement spectrum. The results indicated that the DDBD method is conservative for displacement shapes and storey drifts. Brace ductility results were satisfactory and total shear forces resisted by tension and compression members obtained from NLTHA were found to be greater than the design shear forces as the compression members contributed also in resisting the seismic lateral forces.

An investigation of the forced based design (FBD) approach of CBFs is carried out using the methodology outlined in EC8. Two case studies of 4- and 12-storey CBF buildings are designed using the FBD approach, and then the performance is gauged with NLTH analyses and compared with the DDBD solution. The results showed that FBD approach gives larger section sizes for the same earthquake demand on the building. This leads to lower displacement shapes and storey drifts than the DDBD approach. Moreover, the NLTHA indicated that FBD is conservative for displacement shapes and storey drifts for all storeys except the top floor, which leads to the need of taking into account the higher mode effects on FBD. Total shear forces resisted by tension and compression members obtained from NLTHA were found to be greater than the design shear forces obtained from FBD, as the compression members contributed also in resisting the seismic lateral forces. Thus, this paper highlights benefits of the DDBD approach over the FBD approach for design concentrically braced frames in regions of high seismicity, as it leads to buildings with lower total mass of steel for the case study buildings.

Acknowledgments

This material is in part based upon works supported by the Science Foundation Ireland Marine

Renewable Energy Ireland (MaREI) research centre under Grant No. 12/RC/2302. It was also funded by a fellowship from the College of Engineering and Informatics. The second author would like to acknowledge the support of Science Foundation Ireland through the Career Development Award programme (Grant No. 13/CDA/2200).

References

Besevic, M. (2012), "Experimental investigation of residual stresses in cold formed steel sections", *Steel Compos. Struct., Int. J.*, **12**(6), 465-489. DOI: 10.12989/scs.2012.12.6.465

Calvi, G.M. and Sullivan, T.J. (2009), *A Model Code for the Displacement-based Seismic Design of Structures*, IUSS Press, Pavia, Italy.

CEN (1998), Eurocode 8: Design of structures for earthquake resistance – Part 1: General rules, seismic actions and rules for buildings; EN 1998.

CEN (2004a), Eurocode 1: General actions – Part 1-1: Densities, self-weight, imposed loads for buildings; EN 1991-1-1.

CEN (2004b), Eurocode 8: Design of structures for earthquake resistance – Part 1: General rules, seismic actions and rules for buildings; EN 1998-1:2004/AC: 2009.

CEN (2005), Eurocode 3: Design of steel structures - Part 1-1: General rules and rules for buildings; EN 1993-1-1:2005/AC:2009.

Della Corte, G. and Mazzolani, F.M. (2008), "Theoretical developments and numerical verification of a displacement-based design procedure for steel braced structures", *Proceedings of the 14th World Conference on Earthquake Engineering*, Beijing, China, October.

Della Corte, G., Landolfo, R. and Mazzolani, F.M. (2010), "Displacement-based seismic design of braced steel structures", *Steel Construction*, **3**(3), 134-139. DOI: 10.1002/stco.201010019

Elghazouli, A.Y., Broderick, B.M., Goggins, J., Mouzakis, H., Carydis, P., Bouwkamp, J. and Plumier, A. (2005), "Shake table testing of tubular steel bracing members", *Proceedings of the Institution of Civil Engineers-Structures and Buildings*, **158**(4), 229-241.

Filippou, F.C. and Fenves, G.L. (2004), Methods of analysis for earthquake-resistant structures, (Chapter 6: Earthquake Engineering), From Engineering Seismology to Performance-Based Engineering.

Goggins, J. (2004), *Earthquake Resistant Hollow and Filled Steel Braces*, Doctoral Dissertation, Ph.D. Thesis; Trinity College, University of Dublin, Dublin, Ireland.

Goggins, J. and Salawdeh, S. (2012), "Validation of nonlinear time history analysis models for single-storey concentrically braced frames using full-scale shake table tests", *Earthq. Eng. Struct. Dyn.*, **42**(8), 1151-1170. DOI: 10.1002/eqe.2264

Hu, J.W. (2014), "Seismic analysis and evaluation of several recentering braced frame structures", *Proceedings of the Institution of Mechanical Engineers, Part C: Journal of Mechanical Engineering Science*, **228**(5), 781-798. DOI: 10.1177/0954406213490600

McKenna, F., Fenves, G.L. and Scott, M.H. (2000), Object oriented program, OpenSees; Open system for earthquake engineering simulation. http://opensees.berkeley.edu
Retrieved from http://opensees.berkeley.edu

Medhekar, M.S. and Kennedy, D.J.L. (2000a), "Displacement-based seismic design of buildings—application", *Engineering Structures*, **22**(3), 210-221. DOI: 10.1016/s0141-0296(98)00093-5

Medhekar, M.S. and Kennedy, D.J.L. (2000b), "Displacement-based seismic design of buildings—theory", *Engineering Structures*, **22**(3), 201-209. DOI: 10.1016/s0141-0296(98)00092-3

Moghaddam, H. and Hajirasouliha, I. (2006), "An investigation on the accuracy of pushover analysis for estimating the seismic deformation of braced steel frames", *J. Construct. Steel Res.*, **62**(4), 343-351. DOI: 10.1016/j.jcsr.2005.07.009

Nascimbene, R., Rassati, G.A. and Wijesundara, K.K. (2012), "Numerical simulation of gusset plate connections with rectangular hollow section shape brace under quasi-static cyclic loading", *J. Construct.*

Steel Res., **70**, 177-189. DOI: http://dx.doi.org/10.1016/j.jcsr.2011.09.010
Nip, K.H., Gardner, L., Davies, C.M. and Elghazouli, A.Y. (2010a), "Extremely low cycle fatigue tests on structural carbon steel and stainless steel", *J. Construct. Steel Res*., **66**(1), 96-110. DOI: 10.1016/j.jcsr.2009.08.004
Nip, K.H., Gardner, L. and Elghazouli, A.Y. (2010b), "Cyclic testing and numerical modelling of carbon steel and stainless steel tubular bracing members", *Eng. Struct*., **32**(2), 424-441.
Pennucci, D., Sullivan, T.J. and Calvi, G.M. (2011), "Displacement reduction factors for the design of medium and long period structures", *J. Earthq. Eng*, **15**(sup1), 1-29. DOI: 10.1080/13632469.2011.562073
Priestley, M.J.N., Calvi, G.M. and Kowalsky, M.J. (2007), *Displacement-Based Seismic Design of Structures*, IUSS Press, Pavia, Italy.
Salawdeh, S. (2012), *Seismic Design of Concentrically Braced Frames*, Ph.D., National University of Ireland, Galway, Ireland.
Salawdeh, S. and Goggins, J. (2013), "Numerical simulation for steel brace members incorporating a fatigue model", *Eng. Struct*., **46**, 332-349. DOI: 10.1016/j.engstruct.2012.07.036
SAP2000 (2002), *A General Structural Analysis Program*, Computers and Structures, Inc., University of California, Berkeley, CA, USA.
SeismoSoft (2007), SeismoStruct—A computer program for static and dynamic analysis for framed structures. Available from URL: www.seismosoft.com
Tremblay, R. (2002), "Inelastic seismic response of steel bracing members", *J. Construct. Steel Res*., **58**(5-8), 665-701.
Uriz, P., Filippou, F. and Mahin, S. (2008), "Model for cyclic inelastic buckling of steel braces", *J. Struct. Eng*., **134**(4), 619-628. DOI: 10.1061/(ASCE)0733-9445(2008)134:4(619)
Wijesundara, K.K. (2009), *Design of Concentrically Braced Steel Frames with RHS Shape Braces*, Ph.D. Thesis; ROSE School, IUSS Pavia, Italy, 345 p.
Wijesundara, K.K., Bolognini, D., Nascimbene, R. and Calvi, G.M. (2009), "Review of design parameters of concentrically braced frames with RHS shape braces", *J. Earthq. Eng*., **13**(sup1), 109-131. DOI: 10.1080/13632460902813331
Wijesundara, K.K., Nascimbene, R. and Sullivan, T.J. (2011), "Equivalent viscous damping for steel concentrically braced frame structures", *Bull. Earthq. Eng*., **9**(5), 1535-1558. DOI: 10.1007/s10518-011-9272-4
Wijesundara, K.K., Nascimbene, R. and Rassati, G.A. (2014), "Modeling of different bracing configurations in multi-storey concentrically braced frames using a fiber-beam based approach", *J. Construct. Steel Res*., **101**, 426-436. DOI: http://dx.doi.org/10.1016/j.jcsr.2014.06.009
Yoo, J.-H., Lehman, D.E. and Roeder, C.W. (2008), "Influence of connection design parameters on the seismic performance of braced frames", *J. Construct. Steel Res*., **64**(6), 607-623. DOI: http://dx.doi.org/10.1016/j.jcsr.2007.11.005

CC